Accepted for publication in The Astrophysical Journal
Preprint typeset using LaTeX style emulateapj v. 12/16/11

THE DEPENDENCE OF CONVECTIVE CORE OVERSHOOTING ON STELLAR MASS: SEMI-EMPIRICAL DETERMINATION USING THE DIFFUSIVE APPROACH WITH TWO DIFFERENT ELEMENT MIXTURES

Antonio Claret[1] and Guillermo Torres[2]

Accepted for publication in The Astrophysical Journal

ABSTRACT

Convective core overshooting has a strong influence on the evolution of stars of moderate and high mass. Studies of double-lined eclipsing binaries and stellar oscillations have renewed interest in the possible dependence of overshooting on stellar mass, which has been poorly constrained by observations so far. Here we have used a sample of 29 well-studied double-lined eclipsing binaries in key locations of the H-R diagram to establish the explicit dependence of $f_{\rm ov}$ on mass, where $f_{\rm ov}$ is the free parameter in the diffusive approximation to overshooting. Measurements of the masses, radii, and temperatures of the binary components were compared against stellar evolution calculations based on the MESA code to infer semi-empirical values of $f_{\rm ov}$ for each component. We find a clear mass dependence such that $f_{\rm ov}$ rises sharply from zero in the range 1.2–2.0 $M_{\odot}$, and levels off thereafter up to the 4.4 $M_{\odot}$ limit of our sample. Tests with two different element mixtures indicate the trend is the same, and we find it is also qualitatively similar to the one established in our previous study with the classical step-function implementation of overshooting characterized by the free parameter $\alpha_{\rm ov}$. Based on these measurements we infer an approximate relationship between the two overshooting parameters of $\alpha_{\rm ov}/f_{\rm ov} = 11.36 \pm 0.22$, with a possible dependence on stellar properties.

Keywords: stars: evolution; stars: interiors; stars: core overshooting; stars: eclipsing binaries

1. INTRODUCTION

Theoretical research on the extent of convective cores in stars dates back to the beginning of the 1960's. Convective elements that travel past the boundary of the core as defined by the classical Schwarzschild criterion, and extend its size, give rise to the phenomenon typically referred to as convective core overshooting. The extra mixing has a strong influence on the evolution of stars. It extends their main-sequence lifetimes, and increases the degree of mass concentration towards the center. The latter property can be measured directly by determining the rate of apsidal motion in close, eccentric binary systems (see, e.g., Claret & Giménez 2010). The bibliography on the subject of convective core overshooting is quite extensive, and for the most relevant sources of interest for the present work we refer the reader to our earlier paper on the topic (Claret & Torres 2016, hereafter Paper I).

While it is now widely accepted that core overshooting is needed in order to explain the observations of stars in a variety of stellar populations (see the discussion in the aforementioned paper), the degree to which overshooting might depend on stellar mass has been much less clear. Many (though not all) current grids of stellar evolution models assume some form of mass dependence for the extra mixing, but those prescriptions are largely ad hoc. Empirical support has been scant, and sometimes contradictory. The issue has commonly been addressed most directly using measurements of double-lined eclipsing binaries (DLEBs), and in recent years also using diagnostics from asteroseismology. In the framework of the classical prescription for overshooting the extra distance traveled by the convective elements beyond the limits of the core is represented by $d_{\rm ov} = \alpha_{\rm ov}\ H_p$, where H_p is the pressure scale height and $\alpha_{\rm ov}$ is the classical overshooting parameter. Studies using DLEBs have found results ranging from a strong dependence of the $\alpha_{\rm ov}$ on mass (Ribas et al. 2000) to a more uncertain and much less pronounced dependence (Claret 2007), and even no dependence at all (Meng & Zhang 2014; Stancliffe et al. 2015). The DLEB samples in these investigations have typically been small, not exceeding a dozen or so systems (often far fewer), and have generally been restricted to the main sequence. Asteroseismic studies of single stars have so far been performed over limited ranges in mass and evolutionary state, but do suggest changes in overshooting that are not inconsistent with results described below (see, e.g., Aerts 2013; Deheuvels et al. 2016).

The most comprehensive observational study of the dependence of core overshooting on stellar mass was presented in Paper I, where we made use of a much larger set of 33 DLEBs in the range of 1.2–4.4 $M_{\odot}$ with accurate determinations of their physical properties (masses, radii, effective temperatures, and in many cases metallicities). These systems were carefully selected to be evolved enough so that we could discern the effects of core overshooting and infer a possible dependence on the mass of the star. A clear relation emerged between $\alpha_{\rm ov}$ and stellar mass indicating a steep rise to about 2 $M_{\odot}$ with little or no change beyond this mass. No measurable dependence on metallicity was seen. This semi-empirically determined pattern of overshooting for stars of different mass has found an important practical application for stellar evolution models and has now been incorporated into the new grid of Yale-Potsdam Stellar Isochrones (YaPSI; Spada et al. 2017).

In recent years an alternate prescription for core overshooting has become increasingly popular, in which the

[1] Instituto de Astrofísica de Andalucía, CSIC, Apartado 3004, 18080 Granada, Spain
[2] Harvard-Smithsonian Center for Astrophysics, 60 Garden St., Cambridge, MA 02138, USA

region of convective overshooting is not fully mixed, as in the classical method. Rather, as they travel outwards, the convective elements disintegrate following a diffusive process and the decay of the turbulent velocity field is exponential. Following Freytag et al. (1996) and Herwig et al. (1997), the diffusion coefficient in the overshooting region is given by

$$D_{\rm ov} = D_0 \, \exp\left(\frac{-2z}{H_\nu}\right), \qquad (1)$$

where D_0 is the diffusion coefficient at the convective boundary, z is the geometric distance from the edge of the convective zone, H_ν is the velocity scale height at the convective boundary expressed as $H_\nu = f_{\rm ov}\ H_p$, and the coefficient $f_{\rm ov}$ is a free parameter governing the width of the overshooting layer.

Comparisons between models using both approximations to overshooting over limited ranges in mass indicate the resulting internal structures are rather similar (e.g., Herwig et al. 1997; Noels et al. 2010; Magic et al. 2010), suggesting perhaps a rough scaling between $\alpha_{\rm ov}$ and $f_{\rm ov}$. However, some asteroseismic studies claim to be able to distinguish the internal structures from both types of models, implying they are in fact not quite the same. For example, Moravveji et al. (2015, 2016) find evidence that the diffusive formulation of overshooting seems better able to explain the observed pattern of period spacings of slowly pulsating B stars than the classical step-function formulation.

The "equivalence" between $\alpha_{\rm ov}$ and $f_{\rm ov}$ has yet to be explored more fully over a wide range of masses and evolutionary states. While a calibration of $\alpha_{\rm ov}$ with stellar mass now exists (Paper I), the precise quantitative dependence of $f_{\rm ov}$ with mass is not known at the present time, as has been pointed out by Magic et al. (2010), although one might expect it to be at least qualitatively similar. One of the recent series of publicly available evolutionary models that uses the diffusive approximation for overshooting is the large grid of MESA Isochrones and Stellar Tracks (MIST) by Choi et al. (2016), which is based on the Modules for Experiments in Stellar Astrophysics package (MESA; Paxton et al. 2011, 2013, 2015). These models assume $f_{\rm ov}$ is independent of stellar mass, and adopt a fixed value of $f_{\rm ov} = 0.016$ for all stars with convective cores, tuned to reproduce the shape of the main-sequence turnoff in the color-magnitude diagram (CMD) of the open cluster M67. If $f_{\rm ov}$ actually varies with mass in some fashion, as we expect, the impact of using a constant $f_{\rm ov}$ rather than a mass-dependent one may not be immediately obvious in fitting isochrones to CMDs because of the various degeneracies and uncertainties involved.[3] On the other hand, DLEBs with well measured parameters may provide more sensitive tests.

Without access to an empirical calibration of the mass dependence of $f_{\rm ov}$, modelers wishing to use the now more common diffusive approximation are left with little choice but to adopt a fixed value of this parameter constrained in some way by observations, as in the case just described, or to fall back on artificial trends informed perhaps by theoretical expectations (see also Magic et al. 2010). This unsatisfactory situation provides the main motivation for our work, which is to explore the dependence of overshooting on stellar mass using the diffusive formulation, by means of DLEBs, much in the same way as we did in Paper I with the simpler step-function prescription. Our hope is that the results may provide an empirical basis for a more realistic implementation of diffusive convective core overshooting in future models of stellar evolution. An additional goal is to extend our earlier work and examine the impact on the results of the element mixture and the primordial helium abundance, which lead to differences in the opacities.

The paper is structured as follows: In Section 2 we present our observational sample consisting of 29 well-studied DLEBs. Section 3 describes the new prescription for overshooting we use here, the stellar evolution code, and our methodology to derive for each star the semi-empirical values of $f_{\rm ov}$ and the mixing length parameters $\alpha_{\rm MLT}$, as well as the system metallicity. Our results on the mass dependence of $f_{\rm ov}$ are reported in Section 4 for two different element mixtures, and a general discussion of the results is given in Section 5. We summarize our findings in Section 6. Finally, in Appendix A we use a simple analytical model based on homology transformations and the differential equations of stellar structure to investigate the role of opacities, the equation of state, and nuclear energy generation rates on the enlargement of the convective core due to overshooting. This provides important insight into the behavior of $f_{\rm ov}$ as a function of mass reported in Section 4.

2. OBSERVATIONAL SAMPLE

In our earlier study of Paper I (Claret & Torres 2016) we had assembled a set of 33 detached eclipsing binary systems with well determined masses and radii (typically good to 3% or better) selected so that they are sufficiently evolved for the effects of overshooting to be noticeable. Many of the more evolved systems belong to the Large or Small Magellanic Clouds (LMC, SMC), and are preferentially more massive and more metal-poor than systems from the solar neighborhood, which tend to have compositions near solar. Four of those field binaries, χ^2 Hya, YZ Cas, V885 Cyg, and VV Crv, did not quite meet the requirement adopted there that the individual ages inferred for the components from a comparison with stellar evolution models be within 5% of each other. They were nevertheless retained in that study because their mass ratios are very different from unity and therefore provide stronger leverage for the model fits.

The sample selected for the present work draws heavily on the same set of binaries, though with a few differences. One of the problematic systems, V885 Cyg, now provides satisfactory fits to the models used here within the 5% cap on the age difference, and has been included. This is likely the result of the use of a different stellar evolution code than in Paper I, as described in the next section. On the other hand, for HY Vir (another system with dissimilar masses) we now find poor fits to the models employed for this work, and we have therefore preferred to exclude it. This binary and the three others dropped from the sample in Paper I are interesting in their own right, and a full investigation of the reasons for the poor fits, which may possibly provide further insights into the

[3] In an extreme example of this degeneracy, Michaud et al. (2004) have shown that the CMD of M67 can be well fit even *without* overshooting, if diffusion is included (see also Viani & Basu 2017).

models, will be the subject of a future paper.

The final sample for this work contains 29 DLEBs. Additionally, in a few cases with primary and secondary masses that are indistinguishable within the uncertainties, the use of different models here than in Paper I has led to a different conclusion regarding which component of the system is more evolved. For the benefit of the reader Table 1 lists the properties of the 29 systems we use for this analysis, with the binaries arranged in order of decreasing primary mass and the more evolved star given on the first line.

3. STELLAR MODELS AND FITTING METHODS

In the classical formalism for convective core overshooting, sometimes referred to as the "step-function" approximation, the region beyond the core boundary as specified by the Schwarzschild criterion is assumed to be fully mixed. This simple prescription has found wide application in many of the current series of stellar evolution models, and a calibration of $\alpha_{\rm ov}$ as a function of stellar mass was presented in Paper I.

For the present work we have explored an alternate, exponentially decaying formulation for overshooting that is becoming more common, and is characterized by the free parameter $f_{\rm ov}$ described earlier that determines the width of the overshooting layer. The temperature gradient in this region is assumed to be radiative, and we adopt equal $f_{\rm ov}$ values above the hydrogen and helium burning regions. As mentioned before, recent evidence from an asteroseismic study of the slowly rotating pulsating B stars KIC 10526294 and KIC 7760680 by Moravveji et al. (2015, 2016) indicates this prescription appears to be favored over the classical one, at least in these two cases.[4]

While our previous work in Paper I made use of the Granada stellar evolution code (Claret 2004), the diffusive formulation for overshooting is not yet implemented in that code, so for the present study evolutionary tracks were computed instead with the MESA code (Paxton et al. 2011, 2013, 2015), version 7385. A general description of the input physics of the MESA code is given in the above sources. For stars with convective envelopes we employed the standard mixing-length formalism (Böhm-Vitense 1958), where $\alpha_{\rm MLT}$ is a free parameter.[5] The third-degree equation relating the temperature gradients was solved using the Henyey option in MESA. Microscopic diffusion was included, and the condition to determine the edge of the convection zone is the Schwarzschild criterion. As we did in our earlier work, our evolutionary calculations begin at the pre-main-sequence phase. We have not considered stellar rotation in these models, and mass loss was taken into account with the prescription by Reimers (1977) with the efficiency coefficient set to $\eta = 0.2$. We note, though, that the effects of mass loss in our sample are hardly significant, amounting to no more than 1% of the initial mass for our most massive giants (i.e., at the level of the observational errors in the masses). The high-temperature opacities were taken from the tables by Iglesias & Rogers (1996), and for lower temperatures we used the tables of Ferguson et al. (2005).

In our earlier study we had adopted the element mixture of Grevesse & Sauval (1998), which results in a present-day solar metallicity of $Z_\odot = 0.0189$. The primordial helium content was set to $Y_p = 0.24$, and the adopted slope for the Galactic enrichment law was $\Delta Y/\Delta Z = 2.0$. For the present work we have chosen to use the same element mixture initially to facilitate the comparison, but we also used the more recent mixture of Asplund et al. (2009), for which $Z_\odot = 0.0134$, to explore the effect of a change in opacities. This new mixture was paired with an enrichment law specified by $Y_p = 0.249$ (Planck Collaboration 2016) and a slope $\Delta Y/\Delta Z = 1.67$. Thus, we performed two sets of independent calculations:

- GS98 set: Grevesse & Sauval (1998) mixture, $Y_p = 0.24$, $\Delta Y/\Delta Z = 2.0$ (same as Paper I);
- A09 set: Asplund et al. (2009) mixture, $Y_p = 0.249$, $\Delta Y/\Delta Z = 1.67$.

These choices allow for two comparisons of interest: (1) to study the results from the two different overshooting formulations by comparing the GS98 set with the results of Paper I, which used the classical step-function approximation with same mixture and helium enrichment law; and (2) to explore the influence of the element mixture and the helium content on overshooting using the same (diffusive) prescription for the phenomenon.

The fitting procedure applied here to infer the amount of overshooting for each star and the optimal abundance for each system is similar to the one used in Paper I, as described below. The observational constraints are the measured masses (M), radii (R), and effective temperatures ($T_{\rm eff}$). The best match was sought between these observations and evolutionary tracks calculated for the measured masses of each component, allowing $f_{\rm ov}$ and $\alpha_{\rm MLT}$ to vary freely for each star, and letting Z also be variable but assumed to be the same for the two stars. As only about half of our systems have a measured chemical composition, we have preferred to use that information as a consistency check rather than a strict constraint.

For this work we have again opted for the mixed approach applied in our earlier study that combines a relatively coarse grid search of parameter space with manual fine tuning to arrive at the final best-fit values. The manual adjustment has the advantage over a far more computationally expensive fine grid search that the solutions are easily inspected at each step of the process to avoid inconsistencies in the location of the components in the temperature-radius diagram. This is particularly valuable in rapid phases of evolution that could lead to unphysical situations (e.g., the more massive star being less evolved). For Paper I we had computed a grid of evolutionary tracks spanning a range of $\alpha_{\rm ov}$ values from 0.00 to 0.40 in steps of 0.05, and $\alpha_{\rm MLT}$ values between 1.0 and 2.0 (extended in some cases up to 2.7) with a step of 0.1. We have reused this grid here, not for actual fits but only in a differential sense, to gauge the direction in which predicted stellar parameters (temperature, radius, age) change as the overshooting or mix-

[4] With the present list of binaries we are not able to determine whether one formalism is better than the other. A sample with more direct information on the stellar interiors would be needed, as could be supplied by accurate measurements of apsidal motion in eccentric systems.

[5] The value of the mixing length parameter for the Sun in these models, with the same input physics as used here, is $\alpha_{\rm MLT} = 1.84$ (see Torres et al. 2015).

Table 1
Binaries systems in our sample.

Name	Mass ($M_\odot$)	Radius ($R_\odot$)	$T_{\rm eff}$ (K)	[Fe/H]	Source
SMC-108.1-14904	4.429 ± 0.037	64.05 ± 0.50	4955 ± 90	−0.80 ± 0.15	1
	4.416 ± 0.041	46.95 ± 0.53	5675 ± 105		
OGLE-LMC-ECL-CEP-0227	4.165 ± 0.032	34.92 ± 0.34	6050 ± 160		2
	4.134 ± 0.037	44.85 ± 0.29	5120 ± 130		
OGLE-LMC-ECL-06575	4.152 ± 0.030	39.79 ± 1.35	4903 ± 72	−0.45 ± 0.10	3
	3.966 ± 0.032	49.35 ± 1.45	4681 ± 77		
OGLE-LMC-ECL-CEP-2532	3.90 ± 0.10	28.95 ± 1.4	6345 ± 150		4
	3.83 ± 0.10	37.7 ± 1.7	4800 ± 220		
LMC-562.05-9009	3.70 ± 0.03	28.6 ± 0.2	6030 ± 150:		5
	3.60 ± 0.03	26.6 ± 0.2	6030 ± 150:		
OGLE-LMC-ECL-26122	3.593 ± 0.055	32.71 ± 0.51	4989 ± 80	−0.15 ± 0.10	3
	3.411 ± 0.047	22.99 ± 0.48	4995 ± 81		
OGLE-LMC-ECL-01866	3.574 ± 0.038	46.96 ± 0.61	4541 ± 85	−0.70 ± 0.10	3
	3.575 ± 0.028	28.20 ± 1.06	5327 ± 72		
OGLE-SMC-113.3-4007	3.561 ± 0.025	48.4 ± 0.7	4813 ± 100		6
	3.504 ± 0.028	45.8 ± 0.7	4800 ± 100		
OGLE-LMC-ECL-10567	3.345 ± 0.040	25.6 ± 1.6	5067 ± 73	−0.81 ± 0.20	3
	3.183 ± 0.038	36.0 ± 2.0	4704 ± 80		
OGLE-LMC-ECL-09144	3.303 ± 0.028	26.18 ± 0.31	5288 ± 81	−0.23 ± 0.10	3
	3.208 ± 0.026	18.64 ± 0.30	5470 ± 96		
OGLE-051019.64-685812.3	3.278 ± 0.032	26.05 ± 0.29	5300 ± 100		7
	3.179 ± 0.029	19.76 ± 0.34	5450 ± 100		
OGLE-LMC-ECL-09660	2.988 ± 0.018	43.87 ± 1.14	4677 ± 75	−0.44 ± 0.10	3
	2.969 ± 0.020	23.75 ± 0.66	5352 ± 70		
SMC-101.8-14077	2.835 ± 0.055	23.86 ± 0.31	5170 ± 90	−1.01 ± 0.15	1
	2.725 ± 0.034	17.90 ± 0.50	5580 ± 95		
α Aur	2.5687 ± 0.0074	11.98 ± 0.57	4970 ± 50	−0.04 ± 0.06	8
	2.4828 ± 0.0067	8.83 ± 0.33	5730 ± 60		
WX Cep	2.533 ± 0.050	3.996 ± 0.030	8150 ± 250		7
	2.324 ± 0.045	2.712 ± 0.023	8900 ± 250		
V1031 Ori	2.468 ± 0.018	4.323 ± 0.034	7850 ± 500		7
	2.281 ± 0.016	2.978 ± 0.064	8400 ± 500		
V364 Lac	2.333 ± 0.014	3.309 ± 0.021	8250 ± 150		7
	2.295 ± 0.024	2.986 ± 0.020	8500 ± 150		
SZ Cen	2.311 ± 0.026	4.556 ± 0.032	8100 ± 300		7
	2.272 ± 0.021	3.626 ± 0.026	8380 ± 300		
OGLE-LMC-ECL-25658	2.230 ± 0.019	27.57 ± 0.24	4721 ± 75	−0.63 ± 0.10	9
	2.229 ± 0.019	21.41 ± 0.15	4860 ± 70		
V885 Cyg	2.228 ± 0.026	3.387 ± 0.026	8150 ± 150		7
	2.000 ± 0.029	2.346 ± 0.017	8375 ± 150		
AI Hya	2.140 ± 0.038	3.916 ± 0.031	6700 ± 60		7
	1.973 ± 0.036	2.767 ± 0.019	7100 ± 65		
AY Cam	1.905 ± 0.040	2.772 ± 0.020	7250 ± 100		7
	1.709 ± 0.036	2.026 ± 0.017	7395 ± 100		
SMC-130.5-04296	1.854 ± 0.025	25.44 ± 0.25	4912 ± 80	−0.88 ± 0.15	1
	1.805 ± 0.027	46.00 ± 0.35	4515 ± 75		
OGLE-LMC-ECL-03160	1.799 ± 0.028	37.42 ± 0.52	4490 ± 82	−0.48 ± 0.20	3
	1.792 ± 0.027	16.36 ± 1.06	4954 ± 83		
EI Cep	1.7716 ± 0.0066	2.897 ± 0.048	6750 ± 100		7
	1.6801 ± 0.0062	2.330 ± 0.044	6950 ± 100		
SMC-126.1-00210	1.674 ± 0.037	43.52 ± 1.02	4480 ± 70	−0.86 ± 0.15	1
	1.669 ± 0.039	39.00 ± 0.98	4510 ± 70		
HD 187669	1.505 ± 0.004	22.62 ± 0.50	4330 ± 70	−0.25 ± 0.10	10
	1.504 ± 0.004	11.33 ± 0.28	4650 ± 80		
OGLE-LMC-ECL-15260	1.426 ± 0.022	42.17 ± 0.33	4320 ± 81	−0.47 ± 0.15	3
	1.440 ± 0.024	23.51 ± 0.69	4706 ± 87		
AI Phe	1.2336 ± 0.0045	2.932 ± 0.048	5010 ± 120	−0.14 ± 0.10	7
	1.1934 ± 0.0041	1.818 ± 0.024	6310 ± 150		

Note. — The first line for each system corresponds to the more evolved star. Temperatures for LMC-562.05-9009 are listed as uncertain in the original source. The [Fe/H] value adopted here for OGLE-LMC-ECL-25658 is the average of the individual estimates reported. Sources are: (1) Graczyk et al. (2014); (2) Pilecki et al. (2013); (3) Pietrzyński et al. (2013); (4) Pilecki et al. (2015); (5) Gieren et al. (2015); (6) Graczyk et al. (2012); (7) Torres et al. (2010); (8) Torres et al. (2015); (9) Elgueta et al. (2016); (10) Hełminiak et al. (2015).

ing length are modified, and aid our manual search for better fits. As the relevant variable for this work is $f_{\rm ov}$ rather than $\alpha_{\rm ov}$, we assumed a rough scaling between the two (see also Section 5.1) such that $\alpha_{\rm ov}/f_{\rm ov} \approx 10$ (e.g., Herwig et al. 1997; Noels et al. 2010), and used it to relabel our coarse grid in terms of $f_{\rm ov}$, which we then used as indicated above to guide our solutions. Based on this information and initial estimates of $f_{\rm ov}$, $\alpha_{\rm MLT}$, and Z we computed finer grids of MESA models with the diffusive overshooting approximation over shorter ranges tailored to each system. Small manual adjustments to the parameters were made in the final approach to the optimal fits until the predicted effective temperatures and radii agreed with the measured values approximately within their uncertainties, requiring also that the binary components have a similar age. To account for imperfections in the models and for observational errors, we allowed the derived ages to differ by up to 5%. Satisfactory fits with this condition were found for all 29 of our DLEBs. Initial estimates for Z were based on the measured metallicities for the 16 systems that have them, and for those that do not we used photometric estimates in some cases, or even values from the literature derived from fits to stellar evolution models, if available. We found that the final best-fit Z values occasionally deviated significantly from the initial values, as we discuss later.

Average uncertainties in $f_{\rm ov}$, which we adopt as 0.004 for unevolved stars (dwarfs) and 0.003 for giants, were estimated by varying this parameter keeping $\alpha_{\rm MLT}$ and the chemical composition fixed, with the requirement that the predicted radii and temperatures of the binary components be within the observational uncertainties and that the age difference be no larger than 5%. While these errors are considerably more conservative than those sometimes seen in the literature, we believe them to be realistic. The larger estimate for dwarfs reflects the lower sensitivity to overshooting on the main sequence. A similar procedure was followed for $\alpha_{\rm MLT}$, examining the effect of changes at constant values of $f_{\rm ov}$ and the chemical composition. The uncertainties in $\alpha_{\rm MLT}$ are estimated to be 0.20.

4. RESULTS

As a sanity check on our methods we chose the well-studied case of Capella (α Aur) to generate a grid of evolutionary tracks varying $f_{\rm ov}$ over the range 0.000–0.025 in increments of 0.005, and stepping $\alpha_{\rm MLT}$ over the range from 1.7 and 1.9 every 0.1, bracketing previous determinations for the components that used the same MESA code (see Torres et al. 2015). The observationally well constrained Z value from the same study was held fixed. In addition to verifying that a grid search in this unambiguous case yielded essentially the same answer as our manual method, the exercise also supports our adopted uncertainties in $f_{\rm ov}$ and $\alpha_{\rm MLT}$.

The results of our calculations for the GS98 mixture are presented in Table 2 with the systems listed in the same order as in Table 1, and include the inferred values of the overshooting and mixing length parameters ($f_{\rm ov}$, $\alpha_{\rm MLT}$) for each component, as well as the optimal abundance Z and mean age for each system. Table 3 contains the corresponding results for the A09 mixture. Representative fits for four of our systems are shown in Fig. 1, with the top row corresponding to the GS98 set and the bottom row to A09. The morphology of the evolutionary tracks as well as the inferred evolutionary state of the components is quite similar for the two mixtures.

The behavior of $f_{\rm ov}$ for each element mixture as a function of stellar mass is displayed in Fig. 2, in which the size of the symbols is proportional to the surface gravity $\log g$. All systems more massive than about 2.5 $M_\odot$ are giants. To avoid clutter we show the mean error bars for evolved and unevolved systems on the lower right, rather than on each point.

We find a clear dependence of the overshooting parameter on mass for both mixtures, with a strong rise in $f_{\rm ov}$ up to about 2 $M_\odot$ that flattens out thereafter. This represents the first semi-empirical mass calibration of $f_{\rm ov}$. We defer a discussion of the nature of this relation until Section 5.2. The trend appears qualitatively similar for GS98 and A09, though there may be slight differences. For example, if we consider the regime of stars more massive than 2 $M_\odot$, where $f_{\rm ov}$ is effectively constant, we find an average overshooting parameter for the sample of $f_{\rm ov} = 0.0181 \pm 0.0003$ for the GS98 set (mean of estimates for 40 stars) and $f_{\rm ov} = 0.0164 \pm 0.0003$ for the A09 set.[6] While these appear statistically distinct, the formal uncertainties do not include possible systematic errors, which are difficult to quantify and may be much larger than the statistical errors, so we hesitate to conclude there is a real difference.

Concerning our fitted $\alpha_{\rm MLT}$ values, which rely on the 1-D MESA code, we find that they are in reasonable agreement with the predictions from 3-D radiative hydrodynamic simulations by Magic et al. (2015) restricted to the same range of metallicities, effective temperatures, and surface gravities as the binaries in our sample. This is noteworthy considering the significant differences between the input physics of the MESA code and the 3-D models of Magic et al., and the presence of observational errors in our own estimates.

We note also that the model comparisons with the GS98 mixture lead to best-fit Z values that are on average slightly but systematically smaller than the measured abundances, for the 16 systems for which empirical metallicity estimates are available. A similar but more pronounced effect was seen in Paper I, and is most obvious for some of the metal-poor systems in the LMC and SMC. The average disagreement is at about the 2σ level, corresponding to a [Fe/H] difference of 0.11 ± 0.05 dex. We see no such discrepancy on average with the A09 mixture (Δ[Fe/H] $= 0.02 \pm 0.05$ dex). Possible explanations for the difference in behavior may be related to the opacities themselves, an incorrect slope $\Delta Y/\Delta Z$, or an inaccurate value for the adopted primordial helium content for the GS98 mixture. We return to this in the next section.

5. DISCUSSION

5.1. *The diffusive and step-function implementations of overshooting compared*

A first interesting conclusion we draw from the results is that the qualitative way in which the strength of the overshooting depends on stellar mass (Fig. 2) seems es-

[6] This later value happens to be similar to the one adopted in the MIST grid (Choi et al. 2016) for *all* stars, regardless of their mass.

Table 2
Fitted parameters for our sample of DLEBs using the GS98 mixture.

Name	Primary		Secondary		Z	Mean age (Myr)
	f_{ov}	α_{MLT}	f_{ov}	α_{MLT}		
SMC-108.1-14904	0.0210	1.80	0.0200	1.85	0.0025	130
OGLE-LMC-ECL-CEP-0227	0.0180	2.22	0.0180	2.26	0.0018	139
OGLE-LMC-ECL-06575	0.0190	2.05	0.0180	2.15	0.0080	160
OGLE-LMC-ECL-CEP-2532	0.0170	2.10	0.0200	1.90	0.0022	163
LMC-562.05-9009	0.0150	2.30	0.0150	2.30	0.0025	198
OGLE-LMC-ECL-26122	0.0190	1.80	0.0170	2.13	0.0080	235
OGLE-LMC-ECL-01866	0.0150	2.10	0.0150	2.10	0.0070	229
OGLE-SMC-113.3-4007	0.0205	2.30	0.0205	2.34	0.0035	224
OGLE-LMC-ECL-10567	0.0200	2.12	0.0180	2.00	0.0045	254
OGLE-LMC-ECL-09144	0.0150	2.10	0.0180	1.80	0.0035	252
OGLE-051019.64-685812.3	0.0190	2.40	0.0140	2.40	0.0045	275
OGLE-LMC-ECL-09660	0.0180	2.06	0.0180	2.06	0.0035	341
SMC-101.8-14077	0.0160	2.25	0.0160	2.28	0.0020	366
α Aur	0.0200	1.85	0.0200	1.80	0.0150	608
WX Cep	0.0160	1.85	0.0190	1.85	0.0220	523
V1031 Ori	0.0208	1.85	0.0190	1.85	0.0185	608
V364 Lac	0.0200	1.85	0.0200	1.85	0.0185	611
SZ Cen	0.0195	1.85	0.0190	1.85	0.0090	653
OGLE-LMC-ECL-25658	0.0181	2.06	0.0181	2.05	0.0045	805
V885 Cyg	0.0190	1.85	0.0180	1.85	0.0130	712
AI Hya	0.0160	1.80	0.0180	1.80	0.0370	897
AY Cam	0.0165	1.80	0.0165	1.80	0.0175	970
SMC-130.5-04296	0.0120	2.32	0.0150	2.04	0.0015	983
OGLE-LMC-ECL-03160	0.0800	1.94	0.0080	2.15	0.0025	1023
EI Cep	0.0130	1.90	0.0130	1.90	0.0150	1309
SMC-126.1-00210	0.0120	2.00	0.0120	2.05	0.0020	1240
HD 187669	0.0090	1.80	0.0090	1.82	0.0100	2330
OGLE-LMC-ECL-15260	0.0050	2.00	0.0050	2.11	0.0030	2143
AI Phe	0.0000	1.78	0.0000	2.05	0.0120	4383

Table 3
Fitted parameters for our sample of DLEBs using the A09 mixture.

Name	Primary		Secondary		Z	Mean age (Myr)
	f_{ov}	α_{MLT}	f_{ov}	α_{MLT}		
SMC-108.1-14904	0.0190	1.80	0.0190	1.80	0.0018	123
OGLE-LMC-ECL-CEP-0227	0.0150	1.95	0.0150	2.08	0.0022	138
OGLE-LMC-ECL-06575	0.0170	2.02	0.0170	2.20	0.0070	155
OGLE-LMC-ECL-CEP-2532	0.0140	2.00	0.0170	1.97	0.0021	155
LMC-562.05-9009	0.0132	2.35	0.0128	2.35	0.0025	188
OGLE-LMC-ECL-26122	0.0190	1.80	0.0170	2.13	0.0070	234
OGLE-LMC-ECL-01866	0.0150	2.10	0.0150	2.10	0.0070	229
OGLE-SMC-113.3-4007	0.0161	2.22	0.0161	2.22	0.0020	207
OGLE-LMC-ECL-10567	0.0140	2.25	0.0140	2.00	0.0035	233
OGLE-LMC-ECL-09144	0.0145	2.00	0.0175	1.75	0.0040	247
OGLE-051019.64-685812.3	0.0160	2.08	0.0140	2.33	0.0048	271
OGLE-LMC-ECL-09660	0.0170	2.15	0.0170	2.15	0.0035	333
SMC-101.8-14077	0.0150	2.31	0.0150	2.27	0.0020	353
α Aur	0.0200	1.83	0.0200	1.80	0.0120	594
WX Cep	0.0170	1.85	0.0170	1.85	0.0180	537
V1031Ori	0.0180	1.85	0.0180	1.85	0.0190	634
V364 Lac	0.0170	1.85	0.0170	1.85	0.0150	611
SZ Cen	0.0170	1.90	0.0160	1.85	0.0090	655
OGLE-LMC-ECL-25658	0.0170	1.94	0.0170	1.94	0.0025	728
V885 Cyg	0.0175	1.95	0.0170	1.85	0.0130	715
AI Hya	0.0160	1.87	0.0140	1.87	0.0220	956
AY Cam	0.0150	1.83	0.0140	1.83	0.0150	1023
SMC-130.5-04296	0.0100	2.33	0.0140	2.04	0.0012	929
OGLE-LMC-ECL-03160	0.0070	2.13	0.0070	2.13	0.0033	1034
EI Cep	0.0110	1.85	0.0110	1.80	0.0130	1299
SMC-126.1-00210	0.0100	1.95	0.0100	1.95	0.0013	1156
HD 187669	0.0090	1.80	0.0090	1.80	0.0075	2204
OGLE-LMC-ECL-15260	0.0040	2.00	0.0040	2.25	0.0040	2197
AI Phe	0.0000	1.70	0.0000	1.95	0.0090	4108

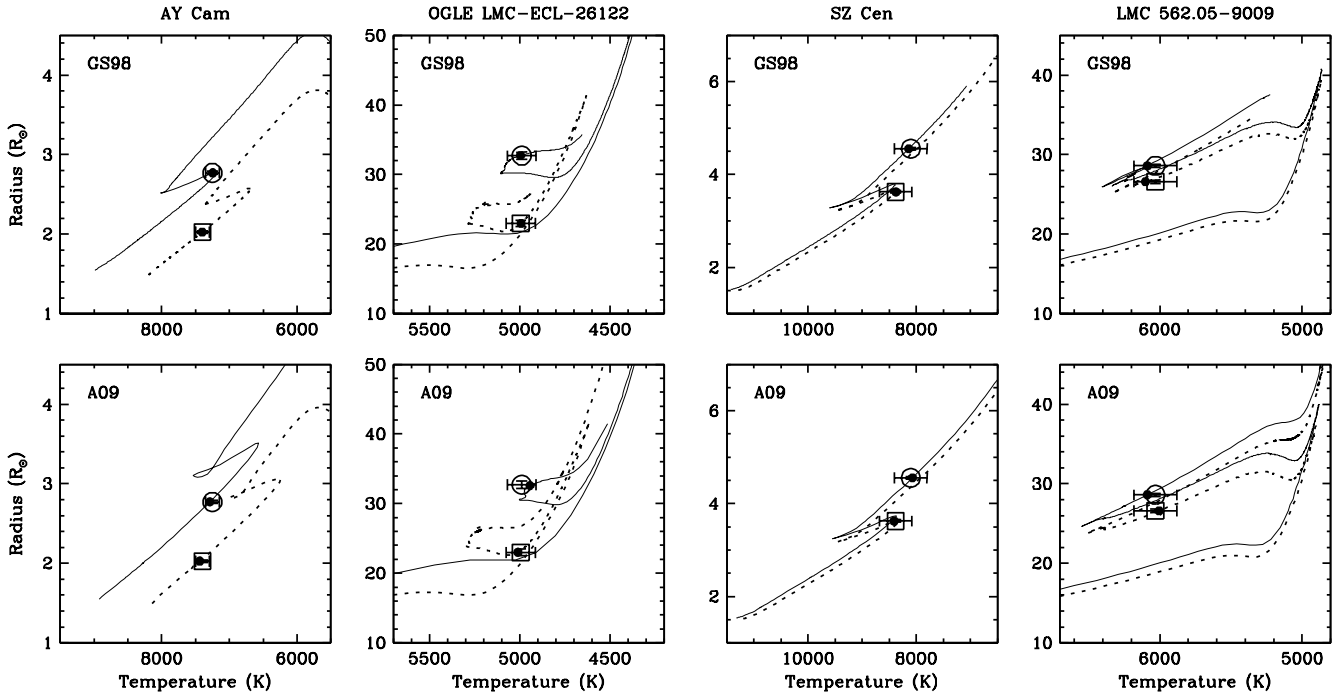

Figure 1. Sample best fits to four of our binaries in the R vs. $T_{\rm eff}$ diagram, for the element mixtures of GS98 (top row) and A09 (bottom row). Evolutionary tracks and the observations for the primary in each system are represented with solid lines and open circles, while dotted lines and open squares are used for the secondary. Small dots mark the best-fit location on each track, and are always within the measurement uncertainties.

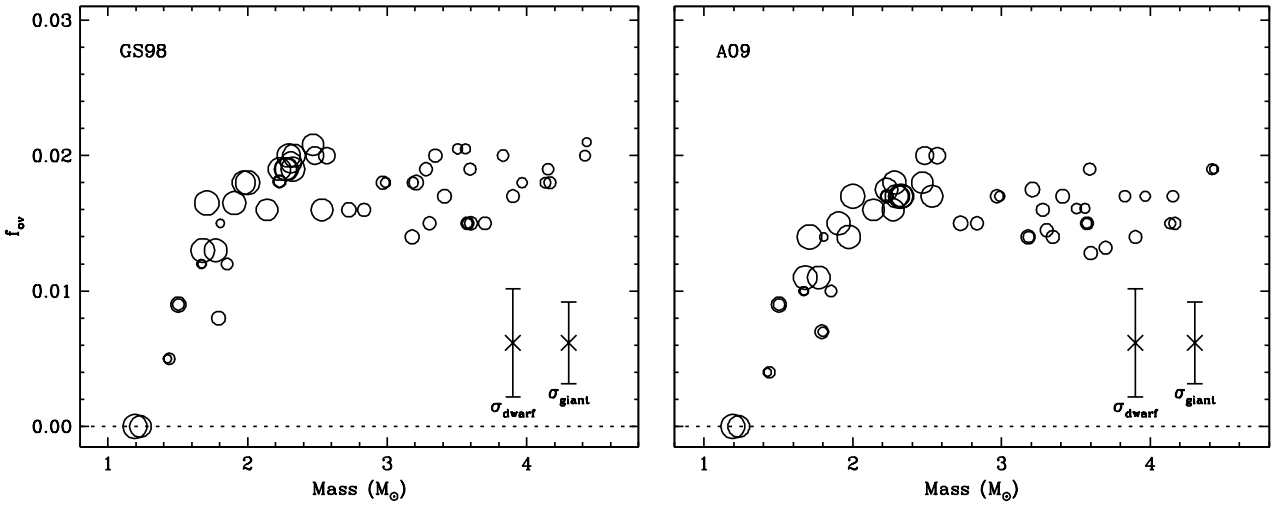

Figure 2. Semi-empirical determinations of the overshooting parameter $f_{\rm ov}$ for both element mixtures, shown as a function stellar mass for the 29 systems in our sample. The size of the points is proportional to $\log g$. Typical uncertainties for dwarfs and giants are represented with the error bars on the lower right.

sentially independent of the opacities and helium enrichment laws involved. Furthermore, the run of $f_{\rm ov}$ with mass from both the GS98 and A09 sets is in turn qualitatively very similar to that obtained in Paper I for $\alpha_{\rm ov}$, which used the step-function approximation. Thus, the details of how the phenomenon is parametrized also seem unimportant, at least when it comes to the mass dependence. While this last conclusion might have been anticipated from the rough similarity between the internal stellar structures inferred theoretically using the two overshooting formulations (e.g., Magic et al. 2010), empirical verification such as we report here remains essential, can lead to further insights, and now provides a practical recipe for incorporating the $f_{\rm ov}$ mass dependence into models, in the same way as our earlier work in Paper I supplied one for the classical $\alpha_{\rm ov}$ implementation. We note, however, that with our current understanding of the phenomenon one recipe cannot necessarily be inferred from the other.

A number of authors (e.g., Herwig et al. 1997; Noels et al. 2010) have in fact suggested an approximate scaling between the two overshooting parameters such that $\alpha_{\rm ov}/f_{\rm ov} \approx 10$, though very few semi-empirical estimates of this relation seem to be available in the literature. One estimate of $\alpha_{\rm ov}/f_{\rm ov} \approx 13$ was reported in an asteroseismic study of the (single) slowly pulsating B star KIC 7760680 by Moravveji et al. (2016). A study of the eclipsing binary TZ For by Valle et al. (2017) gave $\alpha_{\rm ov}/f_{\rm ov} \approx 12$. Magic et al. (2010) made a direct comparison between models for masses ranging from 2 $M_\odot$ to 6 $M_\odot$ using the step-function approximation (with $\alpha_{\rm ov}$ held fixed at 0.20) and calculations based on the diffusive implementation, and obtained a best-fit value with the latter of $f_{\rm ov} = 0.018$, corresponding to a ratio $\alpha_{\rm ov}/f_{\rm ov} \approx 11$. However, their study did not address the more critical regime below 2 $M_\odot$, or stars that have evolved off the main sequence.

A star-by-star comparison between the $f_{\rm ov}$ values from the present work and the $\alpha_{\rm ov}$ values from Paper I (both using the GS98 mixture and the same enrichment law) enables us to revisit this issue. We find that on average $\alpha_{\rm ov}/f_{\rm ov} = 11.36 \pm 0.22$ (mean of 56 ratios, excluding the two stars in AI Phe with $f_{\rm ov} = 0$). This is consistent with previous estimates, but is based on a much larger sample of semi-empirical determinations. The two parameters plotted against each other are shown graphically in Fig. 3. Closer inspection suggests, however, that the connection may be more complex, and there may be a slight dependence of the $\alpha_{\rm ov}/f_{\rm ov}$ ratio on the surface gravity $\log g$, or possibly Z, mass, or $T_{\rm eff}$. Unfortunately these quantities are strongly correlated with each other in our sample. This is because the majority of the cool giants are in the LMC and SMC and are both more massive and significantly more metal-poor than the field dwarfs, so it is not possible to ascertain which variable is the most relevant one. Nonetheless, as an illustration, if we split the sample at $T_{\rm eff} = 6500$ K we obtain averages of $\alpha_{\rm ov}/f_{\rm ov} = 10.50 \pm 0.25$ for the hotter stars and $\alpha_{\rm ov}/f_{\rm ov} = 11.71 \pm 0.27$ for the cooler ones. Identical numbers result for the dwarfs and giants, respectively, if we split the sample at $\log g = 3.0$. The difference is formally at the 3σ level. An even larger sample with a range of uncorrelated stellar properties would be needed to investigate this issue further.

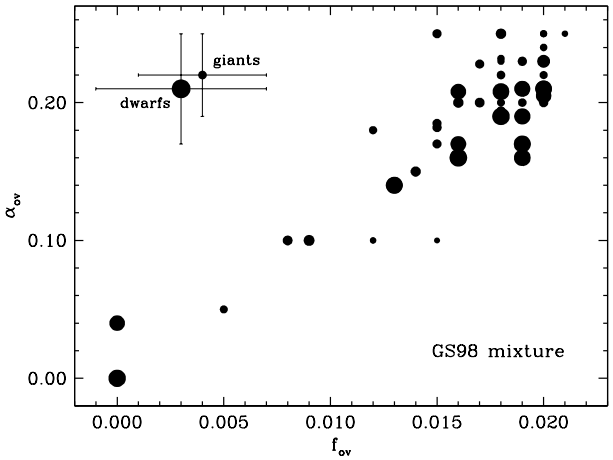

Figure 3. Values of $\alpha_{\rm ov}$ from Paper I shown against the $f_{\rm ov}$ values from this paper. Both use the GS98 mixture. The symbol size is proportional to $\log g$, as in Fig. 2, and representative error bars for evolved and unevolved stars are shown on the upper left.

Overshooting has a significant impact on stellar ages. Between the present work and that of Paper I we now have in hand semi-empirical estimates of the overshooting parameter as well as age estimates derived in the framework of two separate approaches ($f_{\rm ov}$ and $\alpha_{\rm ov}$) for 29 binary systems, using the same element mixture (GS98) and the same helium enrichment law. We find that the mean ages for these 29 systems in common are rather similar for the two overshooting implementations, with an average ratio of Age($f_{\rm ov}$)/Age($\alpha_{\rm ov}$) = 0.975 ± 0.002 (statistical error) and a range of values between 0.88 for AI Phe and 1.10 for OGLE LMC-ECL-26122. Although the mean ratio is formally smaller than unity, we suspect the difference may not be significant given that unquantified systematics probably dominate the error budget, and especially that there are also differences between the Granada and MESA evolutionary codes used in each case, both in terms of their physical ingredients and their numerical details.

5.2. *The size of the convective core and the nature of the mass dependence of $f_{\rm ov}$*

In this section we comment on the underlying reasons for the initial increase in $f_{\rm ov}$ with mass shown in Figure 2, starting around $M \approx 1.2$ $M_\odot$, and the subsequent flattening of the relation after about 2 $M_\odot$ and up to the mass limit of our sample. For this we focus on the behavior of the size of the convective core, as indicated by the models, which is a quantity more closely linked to the interior physics. Using our best-fit values for $f_{\rm ov}$, $\alpha_{\rm MLT}$, and the chemical composition for each star, we have extracted from the corresponding evolutionary tracks the mass of the convective core Q_c that the star has at the zero-age main sequence (ZAMS)[7], which is directly determined by the strength of the overshooting as parametrized by $f_{\rm ov}$. We restrict ourselves to examining the physics at the ZAMS in order to avoid effects from the evolution that occurs later, and because of the simpler, nearly homogeneous chemical structure of

[7] The ZAMS in our models is defined as the location on the H-R diagram at which the central hydrogen content drops to 99.4% of its initial value.

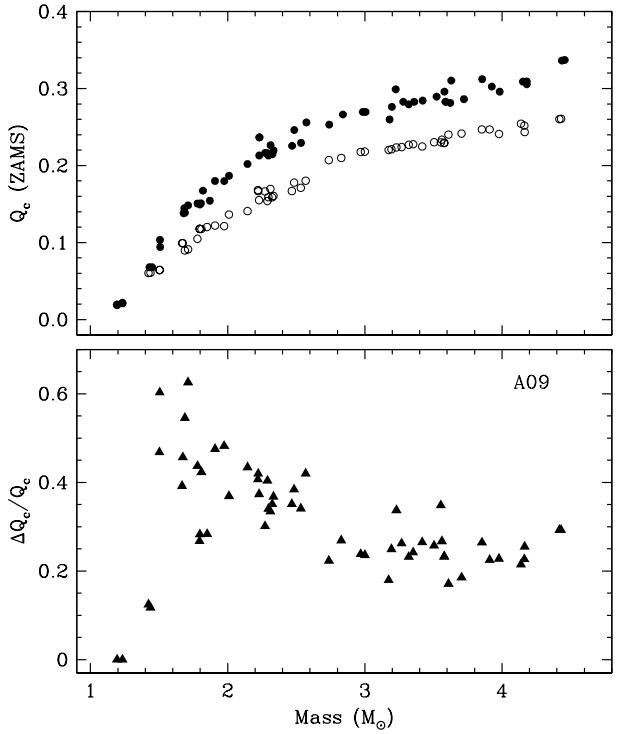

Figure 4. *Top:* Values of the mass Q_c of the convective core (normalized to the total stellar mass) extracted from the best-fit evolutionary track for each star in our sample at the point corresponding to the ZAMS (filled symbols). The results shown are for the A09 mixture; those for the GS98 mixture are similar. The open symbols represent Q_c also at the ZAMS for standard models with no overshooting, at the same chemical composition. The difference in core size between the filled and open symbols that is due to overshooting is seen to vary with stellar mass. *Bottom:* Fractional increase in Q_c between the filled and open circles in the top panel.

ZAMS stars. The top panel of Fig. 5.2 shows how this quantity Q_c, normalized to the total mass of the star, varies as a function of mass for the A09 element mixture in the diffusive approach to overshooting used in this paper (filled symbols). We find a very similar trend for the GS98 mixture (not shown), indicating the opacities have little influence.

The open symbols in the top panel of Fig. 5.2 represent the normalized mass of the convective core at the ZAMS *in the absence of overshooting* (i.e., from "standard" models that use the Schwarzschild criterion to set the core boundary). As before, the results are similar for GS98 and A09. The separation between the filled and open symbols at a given mass represents the enlargement of the convective core due to overshooting. This net growth is seen to increase rapidly with mass up to about 2 $M_\odot$, but not much thereafter, reflecting the same trend observed in Fig. 2. An equivalent representation is displayed in the lower panel of Fig. 5.2, which shows the fractional change in Q_c. For both element mixtures we see an obvious trend such that the fractional increase in Q_c is larger for the less massive stars, reaching ∼60% at about 1.5 $M_\odot$ and then decreasing to 20–30% for the higher mass stars in our sample.

The physical reasons for this behavior of the fractional size of the convective core as a function of stellar mass, with a change in character around 2 $M_\odot$, have to do with concomitant changes in the opacities, the equation of state, and the nuclear reaction rates. We explore this in further detail in the Appendix using a simple analytical toy model involving homology transformations and the basic differential equations of stellar structure. We show there that it is indeed possible to understand the trends in Figures 2 and 5.2 as due at least in part to the role of those ingredients at different masses.

Finally, we note that the way in which Q_c varies with stellar mass is essentially the same as seen in Figure 5 of Paper I for the step-function approximation to overshooting, and similarly with the fractional change in Q_c (Figure 5 of Paper I, lower panel). In the latter case, though, the effect was somewhat magnified because the models without overshooting were computed for a single representative solar metallicity, rather than the Z value of each system that we use in the present work. Thus, once again the formulation of overshooting appears not to matter much in terms of the general trend, at least to first order. This is not entirely surprising given the approximate scaling reported earlier between the two free parameters, $\alpha_{\rm ov} \approx 11.4 f_{\rm ov}$, which to some extent implies a correspondence in the net effect of overshooting even though the details of how it operates in the two implementations are not the same.

5.3. *Relation between the best-fit metallicities and the primordial helium abundance*

In Section 4 we noted that our fitting procedure with the GS98 mixture resulted in a small but systematic difference, on average, between the best-fit abundances and those measured for the 16 binary systems where this is available. The fitted values are slightly smaller, especially for the more metal-poor systems. This is in the same direction as a similar discrepancy noted in Paper I, which explored the classical prescription for overshooting with the same GS98 element mixture and also the same helium enrichment law used here ($Y_p = 0.24$, $\Delta Y/\Delta Z = 2.0$). It was pointed out in our earlier work that the effect could possibly be explained if the measured temperatures for all the binaries were systematically too hot by 150–200 K, though this seemed unlikely.

Interestingly, the abundance discrepancy is not present when using the A09 mixture and an alternate enrichment law specified by $Y_p = 0.249$ and $\Delta Y/\Delta Z = 1.67$. To investigate which, if any, of these two ingredients (mixture, or enrichment law) might be responsible for the metallicity disagreements, we repeated the fits for some of the most obvious outliers that have a measured metallicity, using again the GS98 mixture but this time with the above enrichment law instead of the one indicated in the previous paragraph. We obtained virtually unchanged values for $f_{\rm ov}$, $\alpha_{\rm MLT}$, and the mean system ages, and the resulting best-fit metallicities were now in better agreement with the observations, pointing to the helium abundance as the culprit. More specifically, the improvement is largely the result of the increase in Y_p from 0.24 to 0.249, rather than the change in the slope $\Delta Y/\Delta Z$ from 2.0 to 1.67, because the slope difference has only a minor impact on the total helium abundance for our metal-poor binary systems, which are the ones where the metallicity discrepancy is most noticeable. Similar results were obtained from experiments with the Granada code and the step-function implementation of overshooting using $Y_p = 0.249$, again suggesting a connection with helium. In support of these clues we note that both the radius

and temperature of a given stellar configuration depend on some positive power of the mean molecular weight. A reduction in the hydrogen content of the core implies a larger mean molecular weight, which in turn increases the radius and temperature at a given mass. Thus, at a fixed value of Z, models with the more recent determination of $Y_p = 0.249$ (Planck Collaboration 2016) are hotter, larger, and brighter than those with $Y_p = 0.24$, which explains at least in part why the use of a lower Y_p with the GS98 mixture seemed to imply the empirically measured temperatures were overestimated. We point out, finally, that this realization does not affect the conclusions by Claret & Torres (2016) regarding the mass dependence of $\alpha_{\rm ov}$, or the similar conclusions reported here with the diffusive overshooting formulation and the GS98 mixture. This is because neither the $\alpha_{\rm ov}$ nor the $f_{\rm ov}$ inferences are significantly influenced by the assumed helium abundance as long as Z is allowed to vary in the fits, as has been the case both here and in Paper I.

6. CONCLUDING REMARKS

The key result of this paper is the determination of the explicit dependence of the diffusive convective core overshooting parameter $f_{\rm ov}$ on stellar mass in a semi-empirical way, relying on a set of nearly 30 eclipsing binary systems with well measured properties. This study extends our previous one of Claret & Torres (2016) that used the classical step-function approximation for overshooting with its free parameter $\alpha_{\rm ov}$ and a similar set of binaries, and completes our investigation of the phenomenon with the two most commonly used prescriptions. Additionally, in the present work we have tested two different element mixtures for the opacities, adding to the Grevesse & Sauval (1998) mixture used in Paper I a more recent mixture by Asplund et al. (2009). We find a clear dependence of $f_{\rm ov}$ on stellar mass rising to about 2 $M_\odot$ and then leveling off to the upper mass limit of our sample ($\sim$4.4 $M_\odot$), regardless of the opacities. This qualitative behavior is similar to the one found before for $\alpha_{\rm ov}$. While many recent grids of stellar evolution models build in variations in the strength of overshooting with mass in somewhat arbitrary ways, this study and that in Paper I now provide practical recipes for doing this that are grounded on observations, rather than expectations from theory. Our $f_{\rm ov}$ calibration therefore represents an important step forward, although there is still ample room for improvement before it can be considered definitive. For example, our binary sample has few stars near the low end of the mass range where overshooting begins to ramp up, and about half of the systems are lacking empirical metallicity estimates that could be used to further constrain the fits. Observational errors and shortcomings in the models themselves must also be kept in mind.

We have examined the nature of the mass dependence of $f_{\rm ov}$ by focusing on the related fractional increase in the size of the convective core at the ZAMS ($\Delta Q_c/Q_c$) caused by diffusive overshooting. This quantity is more closely linked to the physics of stellar interiors, and also shows a mass dependence such that stars with smaller masses have larger relative increases in the core mass Q_c up to 60%, which becomes smaller (20–30%) for larger stars. The behavior is similar for both element mixtures used here, and also mirrors that seen in Paper I with the step-function implementation of overshooting. The use of a simple model based on homology transformations and the basic differential equations of stellar structure succeeds in explaining this trend in a qualitative way, revealing the role of opacities, the equation of state, and nuclear reaction rates. A deeper understanding of the behavior of $f_{\rm ov}$ as a function of stellar mass displayed in Figure 2 would benefit from an investigation into the physical conditions at the edge of the convective cores, and how they affect the convective plumes. While such a study is beyond the scope of the present work, we plan to undertake it in a future publication.

Our use of two different helium enrichment laws associated with the adopted GS98 and A09 mixtures has also helped to shed light on a nagging systematic difference between the fitted and measured metallicities noted originally in Paper I, and seen also here with the GS98 set to a lesser degree. We find that the discrepancy is largely removed by adopting the higher primordial helium abundance $Y_p = 0.249$ established in recent studies (Planck Collaboration 2016), instead of the value $Y_p = 0.24$ we used previously.

Comparing our $f_{\rm ov}$ determinations that use the GS98 mixture and the diffusive approximation with the $\alpha_{\rm ov}$ estimates from Paper I based on the step-function prescription and the same mixture (as well as the same enrichment law), we establish a semi-empirical scaling relationship between the two overshooting parameters such that $\alpha_{\rm ov}/f_{\rm ov} = 11.36 \pm 0.22$ (mean of 56 estimates), with a tentative dependence on either temperature or $\log g$, or possibly mass or Z (all strongly correlated in our sample). This connection between $f_{\rm ov}$ and $\alpha_{\rm ov}$ is consistent with, but now more firmly established than previous estimates.

We are grateful to A. Dotter for expert assistance and advice in using the MESA module, as well as C. Aerts for references and helpful comments on the subject of this paper. We also thank our two anonymous referees for constructive criticism. The Spanish MEC (AYA2015-71718-R and ESP2015-65712-C5-5-R) is gratefully acknowledged for its support during the development of this work. GT acknowledges partial support from the NSF through grant AST-1509375. This research has made use of the SIMBAD database, operated at the CDS, Strasbourg, France, and of NASA's Astrophysics Data System Abstract Service.

REFERENCES

Ade, P.A.R., Aghanim, N., Arnaud, M. et al. 2016, A&A, 594, A13
Aerts, C. 2013, in Setting a New Standard in the Analysis of Binary Stars, eds. K. Pavlovski, A. Tkachenko & G. Torres, EAS Publications Series, Vol. 64, 2013, pp. 323-330
Asplund, M., Grevesse, N., Sauval, A. J., & Scott, P. 2009, ARA&A, 47, 481 (A09)
Böhm-Vitense, E. 1958, ZAp, 46, 108
Choi, J., Dotter, A., Conroy, C. et al 2016, ApJ, 823, 102C
Claret, A., Giménez, A. 1991, A&A, 244, 319
Claret, A. 2004, A&A, 424, 919
Claret, A. 2007, A&A, 475, 1019
Claret, A., Giménez, A. 2010, A&A, 519, 57
Claret, A., Torres, G. 2016, A&A, 592, A15 (Paper I)
Deheuvels, S., Brandao, I., Silva Aguirre, V., et al. 2016, A&A, 589A, 93D.
Elgueta, S. S., Graczyk, D., Gieren, W. et al. 2016, AJ, in press
Fekel, F. C., Henry, G. W., & Sowell, J. R. 2013, AJ, 146, 146

Ferguson, J. W., Alexander, D. R., Allard, F., Barman, T., Bodnarik, J. G., Hauschildt, P. H., Heffner-Wong, A., & Tamanai, A. 2005, ApJ, 623, 585
Freytag, B., Ludwig, H.-G., & Steffen, M. 1996, A&A, 313, 497
Gieren, W., Pilecki, B., Pietrzyński, G., et al. 2015, ApJ, 815, 28
Graczyk, D., Pietrzyński, G., Thompson, I. B. et al. 2012, ApJ, 750, 144
Graczyk, D., Pietrzyński, G., Thompson, I. B. et al. 2014, ApJ, 780, 59
Grevesse, N., & Sauval, A. J. 1998, Space Sci. Rev., 85, 161 (GS98)
Hełminiak, K. G., Graczyk, D., Konacki, M., et al. 2015, MNRAS, 448, 1945
Herwig, F., Bloecker, T., Schoenberner, D., & El Eid, M. 1997, A&A, 324, L81
Iglesias, C. A., & Rogers, F. J. 1996, ApJ, 464, 943
Sandberg Lacy, C. H., & Fekel, F. C. 2011, AJ, 142, 185
Magic, Z. Serenelli, A., Weiss, A. et al. 2010, ApJ, 718, 1378
Magic, Z., Weiss, A., & Asplund, M. 2015, A&A, 573, A89
Meng, Y., & Zhang, Q. S. 2014, ApJ, 787, 127
Michaud, G., Richard, O., Richer, J., & VandenBerg, D. A. 2004, ApJ, 606, 452
Moravveji, E., Aerts, C., Pápics, P. I., Triana, S. A., Vandoren, B. 2015, A&A, 580, A27
Moravveji, E., Townsend, R. H. D., Aerts, C., & Mathis, S. 2016, ApJ, 823, 130
Nieuwenhuijzen, H., & de Jagger, C. 1990, A&A, 231, 134
Noels, A., Montalban, J., Miglio, A., Godart, M., & Ventura, P. 2010, Ap&SS, 328, 227
Pavlovski, K., Southworth, J., Kolbas, V., & Smalley, B. 2014, MNRAS, 438, 590
Paxton, B., Bildsten, L., Dotter, A. et al. 2011, ApJS, 192, 3
Paxton, B., Cantiello, M., Arras, P., et al. 2013, ApJS, 208, 4
Paxton, B., Marchant, P., Schwab, J., et al. 2015, ApJS, 220, 15
Pietrzyński, G., Graczyk, D., Gieren, W. et al. 2013, Nature, 495, 76
Pietrzyński, Thompson, I. B., Gieren, W. et al. 2010, Nature, 468, 542
Pilecki, B., Graczyk, D., Pietrzyński, G., et al. 2013, MNRAS, 436, 953
Pilecki, B., Graczyk, D., Gieren, W., et al. 2015, ApJ, 806, 29
Pols, O. R., Tout, C. A., Eggleton P. P., Han, Z. 1995, MNRAS, 274, 964
Reimers, D. 1977, A&A, 61, 217
Ribas, I., Jordi, C., & Giménez, A. 2000, MNRAS, 318, 55
Spada, F., Demarque, P., Kim, Y.-C., Boyajian, T. S., & Brewer, J. M. 2017, AJ, in press (arXiv:1703.03975)
Stancliffe, R. J., Fossati, L., Passy, J.-C., & Schneider, F. R. N. 2015, A&A, 575, 117
Tkachenko, A., Degroote, P., Aerts, C. et al. 2014, MNRAS, 438, 3093
Torres, G., Andersen, J., & Giménez, A. 2010, A&A Rev., 18, 67
Torres, G., Claret, A., Pavlovski, K., & Dotter, A. 2015, ApJ, 807, 26
Torres, G., Vaz, L. P. R., Lacy, C. H. S., & Claret, A. 2014, AJ, 147, 36
Valle, G., Dell'Omodarme, M., Prada Moroni, P. G., & Degl'Innocenti, S. 2017, A&A, 600, A41
Viani, L., & Basu, S. 2017, in Seismology of the Sun and the Distant Stars 2016 (Joint TASC2 & KASC9 Workshop and SPACEINN & HELAS8 Conference), eds. M. J. P. F. G. Monteiro, M. S. Cunha, and J. M. T. Ferreira, EPJ Web of Conferences, in press

APPENDIX

CORE OVERSHOOTING AND HOMOLOGY TRANSFORMATIONS

Here we explore and attempt to understand the nature of the stellar mass dependence of $\Delta Q_c/Q_c$ (the relative change in the core mass shown in the lower panel of Fig. 5.2), which is directly linked to the $f_{\rm ov}$ trend of Fig. 2, as revealed by our semi-empirical estimates for our sample of 29 eclipsing binary systems. We will use simple ideas based on homology transformations, in which the two stellar models to be scaled are required to have the same relative mass distribution. One of the most useful tools to investigate how mass is distributed in stellar interiors is the Radau differential equation, whose solution provides the apsidal-motion constant k_j of order j that gives an accurate indication of the mass distribution. Standard models and those computed with core overshooting for the same mass present similar apsidal-motion constants at the ZAMS, indicating that they also have similar relative mass distributions (see, e.g., Claret & Giménez 1991, Figs. 2, 4, and 6). The same holds when analyzing the properties of the respective cores. Therefore, we may apply homology transformations to both standard homogeneous models as well as those with extra mixing from overshooting. Due to the complexity of the various ingredients of stellar physics (opacities, energy generation, equation of state, etc.) homology transformations do not guarantee accurate solutions, but they are still very useful to explore certain problems in a qualitative way, and even quantitatively to some degree, providing insights into the physics involved.

For the problem at hand —understanding the change in $\Delta Q_c/Q_c$ as a function of stellar mass, which is closely related to the change in $f_{\rm ov}$ as a function of mass— we begin with a star in hydrostatic equilibrium with a convective core of mass Q_0 that satisfies the Schwarzschild criterion, and that is surrounded by a shell of negligible mass in radiative equilibrium. Consider now a second model to be scaled from the first, with a large convective core $Q_0 + \Delta Q$. Our reference shell is displaced upward to a position $R_0 + \Delta R$ simulating the effect of core overshooting. We apply simple homology relations and the basic differential equations of stellar structure and evolution to study in an approximate quantitative way the impact of the increase in radius (and mass) of the convective core.

The net rate of nuclear energy generation inside a sphere of radius r is given by

$$\frac{dL_g(r)}{dr} = 4\pi r^2 \rho \epsilon, \tag{A1}$$

where L_g denotes the rate of energy production by nuclear processes, ϵ is the thermonuclear energy generation rate per unit mass ($\epsilon = b\rho T^\nu$), ρ is the density, T is the temperature, b is a constant, and r is the radial distance. Here we focus on homogeneous (ZAMS) models to compare with the data displayed in Fig. 5.2. Let Q_0, R_0 and μ_0 be the mass, radius, and the mean molecular weight of the standard convective core (without extra mixing) and Q, R, and μ the same variables for a configuration with extra mixing, i.e., with radius $R = R_0 + \Delta R$, core mass $Q = Q_0 + \Delta Q$, and mean molecular weight $\mu = \mu_0 + \Delta\mu$. The homology transformations will be used to scale one model to the other and evaluate the changes ΔQ and ΔR produced by the additional mixing. Inserting the usual homology transformations

for the density and temperature, assuming an ideal non-degenerate gas with no radiation pressure, and integrating the above equation, we obtain

$$L_g(x) = \frac{Q}{Q_0}\int_0^x \left(\frac{b}{b_0}\right)_{x'} \frac{dL_{go}(x')}{dx'}dx' = L_{go}(x)\left(\frac{b}{b_0}\right)\left(\frac{\mu}{\mu_0}\right)^{\nu}\left(\frac{Q}{Q_0}\right)^{2+\nu}\left(\frac{R}{R_0}\right)^{-3-\nu} \tag{A2}$$

where $x = r/R$.

The restriction mentioned above concerning the equation of state is necessary because, even if we consider an ideal gas, the addition of radiation pressure will not lead to permanent homology relationships. On the other hand, as we are dealing with homogeneous models, we may take $\mu = \mu_0$, and we may also assume that the constants b and b_0 are independent of x for small ΔR. In this case, the relative change in the nuclear energy generation will be given by

$$\frac{\Delta L_g}{L_g} = (2+\nu)\frac{\Delta Q}{Q_0} - (3+\nu)\frac{\Delta R}{R_0}. \tag{A3}$$

Additionally, the equation of radiative transfer can be written as

$$\frac{\partial T}{\partial r} = -\frac{3}{16\pi ac}\frac{\kappa\rho L_{\rm rad}}{r^2T^3}, \tag{A4}$$

where $L_{\rm rad}$ is the net rate of energy carried out by radiation, a is the radiation pressure constant, and c is the speed of light. As before, we apply the homology relation for the density assuming a perfect ideal gas, no radiation pressure, and assuming a Kramers complete opacity law given by $\kappa = B\rho^n T^{-s}$, where B is a constant. The same remarks from above concerning b and b_0 hold also for the constants B and B_0. Finally the resulting relative change of energy $L_{\rm rad}$ is

$$\frac{\Delta L_{\rm rad}}{L_{\rm rad}} = (3-n+s)\frac{\Delta Q}{Q_0} - (3n-s)\frac{\Delta R}{R_0}. \tag{A5}$$

We note that the relative change in $L_{\rm rad}$ is insensitive to the rate of nuclear energy generation because it is independent of ν. Under conditions of thermal equilibrium we have $\Delta L_g/L_g = \Delta L_{\rm rad}/L_{\rm rad}$, from which the fractional increase in the convective core mass due to the extra mixing is easily derived as

$$\frac{\Delta Q}{Q_0} = \frac{(3+3n+\nu-s)}{(n+\nu-s-1)}\frac{\Delta R}{R_0}. \tag{A6}$$

Note also that $L_{\rm rad}$ depends only on how energy is transported (opacities, equation of state), whereas L_g depends on how it is generated (thermonuclear energy generation rate per unit mass). The functional form of the slope at each mass in Eq. A6 is the result of the interaction between both processes. This interaction is a consequence of the imposition of the condition of thermal equilibrium. The above equation may also be derived in a different way using permanently homologous models by expanding Q/Q_0 in a series up to 2nd order.

The slope $(3+3n+\nu-s)/(n+\nu-s-1)$ in Eq. A6 presents some interesting features. For pure Thomson scattering or for Kramers opacities it is larger for lower values of ν, that is, for stars for which the proton-proton chain contributes significantly to the energy generation. In other words, the slope is more pronounced for less massive stars than for more massive ones. For larger values of ν the slope has a near-asymptotic behavior, independently of the adopted opacity law.

The dependence on temperature of the two major nuclear sources of energy during the main-sequence (the proton-proton chain and the CNO cycle) shows three main characteristics: (1) for $\log T < 7.25$ the dominant source is the proton-proton chain, (2) for $\log T \approx 7.25$ the two processes have a similar contribution, and (3) for $\log T \approx 7.3$ (corresponding to a stellar mass larger than about 2 $M_\odot$) the CNO cycle contributes about 10 times more than the proton-proton chain, and at a slightly higher temperature of $\log T = 7.4$ it becomes about 100 times more important. Due to the complicated nature of the nuclear energy rates, and the fact that in a given star both nuclear processes may be acting at the same time in different regions, it is difficult to determine an effective value of ν for each mass. It is common to assign a typical value of $\nu = 4$ for stars of small mass and $\nu = 17$ for more massive stars, though without explicitly stating a dependence on mass. To provide a continuous relation between these two regimes for our purposes we adopt a simple linear expression motivated by the properties of the nuclear energy production summarized above, of the form $\nu_{\rm eff} = (M - 1.25) + 4.8$, to be inserted in Eq. A6. In this expression M is the stellar mass in solar units. For simplicity we assume also that the opacity is given by the classical Kramers law ($n = 1$, $s = 7/2$).

With these ingredients we may now compare the relative increase in core mass due extra mixing, as given by Eq. A6, with the semi-empirical data from our 29 DLEBs. As we cannot establish the values of $\Delta R/R_0$ for the binary components a priori (from first principles), we consider a few fixed values and draw iso-$\Delta R/R_0$ curves in Fig. 5 for comparison with the observations. The triangles in this figure represent the semi-empirical values of $\Delta Q_c/Q_c$ for each star obtained using the A09 mixture. We explore three values of $\Delta R/R_0$ as shown by the three curves in the figure (0.15, 0.10, and 0.05, from top to bottom). Detailed estimates of $\Delta R/R_0$ for selected binaries in our sample using the best-fit models give values within this range, indicating they are realistic.

Despite the simplicity of our analytical model, the theoretical iso-$\Delta R/R_0$ curves show a similar pattern of variation as the semi-empirical data, with the less massive stars displaying higher $\Delta Q_c/Q_c$ values than more massive stars.

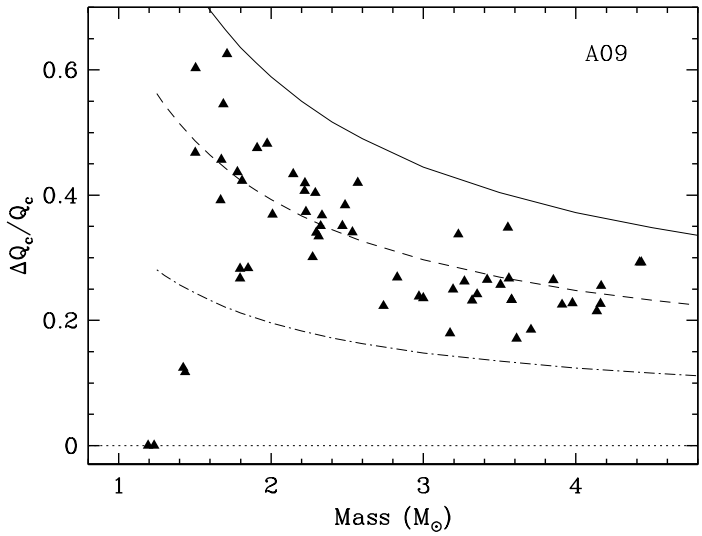

Figure 5. Relative increase in the mass of the convective core as a function of stellar mass. The solid line corresponds to the iso-$\Delta R/R_0$ curve for the value 0.15, the dashed line is for 0.10, and the dot-dashed line for 0.05. Triangles represent the semi-empirical values with the A09 mixture.

Additionally, it can be seen that the previously mentioned near-asymptotic behavior of the slope for the more massive stars is consistent with the semi-empirical results. While these calculations were made specifically for the A09 mixture, we found the same features when using the GS98 set.

In summary, building on very simple approximations Eq. A6 is able to successfully predict the pattern of changes in the relative increase $\Delta Q_c/Q_c$ in the mass of the convective core due to overshooting, illustrating the connection between this slope and stellar mass, the type of nuclear process, the opacities, and the equation of state.